insects

MDPI

Article

Cable Allocation and Reference-Plane Crossings in Sex-Associated Neurons of the Male Drosophila Connectome

Bo-Kyun Kim [1] and Dongsun Shin [2,*]

[1] Department of Paramedicine, College of Medical Science, Gachon University, Incheon 21936, Republic of Korea; victory15xx@gachon.ac.kr
[2] School of AI Convergence, Sehan University, Dangjin 31746, Republic of Korea
* Correspondence: sdssoft@naver.com

Simple Summary

Fruit flies have nerve cells associated with differences between male and female behavior, but these cells do not all distribute their branches in the same way across the two sides of the nervous system. We measured the reconstructed branches of 2368 cells carrying sex-related annotations in a public map of one male fly. Some annotation groups contained many cells with branches almost entirely on one side, whereas others contained more cells extending across both sides. However, the apparent differences also depended on which cell types were common in each group. Giving each type equal weight changed the interpretation of crossing counts. This study provides measurements and reusable code for selecting cells for further investigation. It does not establish differences between male and female flies or demonstrate how these cells control behavior.

Abstract

We aimed to compare cable allocation and reference-plane crossing counts among four sex-associated annotation groups in a single adult male *Drosophila melanogaster* and to assess how cell-type weighting affected the comparison of crossing counts. No female neurons were analyzed. We reanalyzed the electron microscopy-based reconstructions of 2368 neurons in the public male-cns:v1.0 connectome, each carrying one of four source annotations: male-specific (MS), sexually dimorphic (SD), potentially sexually dimorphic (pSD), or potentially male-specific (pMS). The primary measure of cable allocation was the fraction of each neuron's reconstructed length on the side of the plane opposite its annotated soma (C). We also counted reference-plane crossings. Median C was 0.000 in the SD group and 0.128 in the MS group. The comparison of crossing counts depended on how cell types were weighted. When type medians were weighted by neuron count, the SD mean was lower than the MS mean. Giving each type equal weight reversed this ordering. These findings show how cell-type abundance shapes comparisons among annotation groups within this male specimen. Assessing whether these patterns differ between sexes requires matched measurements from additional male and female specimens.

Keywords: *Drosophila melanogaster*; insect neuroanatomy; connectomics; neuronal morphology; hemispheric allocation; midline crossing; fruitless; doublesex

Check for updates

Academic Editor: Victor Benno Meyer-Rochow

Received: 2 October 2026
Revised: 24 November 2026
Accepted: 26 November 2026
Published: 29 November 2026

Copyright: © 2026 by the authors. Licensee MDPI, Basel, Switzerland. This article is an open access article distributed under the terms and conditions of the Creative Commons Attribution (CC BY) license.

1. Introduction

Finding and recognizing a mate requires insects to detect sensory cues and respond with an appropriate action, such as orienting toward a potential partner or initiating

courtship. In the silkmoth *Bombyx mori*, females release the pheromone bombykol, which elicits source-searching behavior in males. Sakurai et al. [1] showed that disrupting the bombykol receptor BmOR1 abolished this behavior and that restoring receptor expression restored the response. This finding identifies a specific sensory mechanism by which a signal from one sex guides mate searching in the other. In *Drosophila melanogaster*, *fruitless* and *doublesex* contribute to the development of neural substrates for sex-specific behavior [2,3]. Anatomical comparisons have identified sex-dependent arborizations in selected neuronal populations, demonstrating that shared cell classes need not have identical projection patterns in males and females [4]. These findings motivate quantitative descriptions of the spatial organization of sex-associated neurons, while also requiring a distinction between anatomical measurements and behavioral function.

Whole-brain reconstruction and systematic cell typing have made neuron-level comparisons possible across large portions of the adult fly brain [5,6]. Berg et al. reconstructed the male central nervous system (CNS) and compared male and female brain connectomes to identify corresponding cell types and characterize sex-related differences in morphology and connectivity [7]. Here, we use the annotations from that study to ask how individual neurons distribute their cable across a soma-referenced coordinate plane and how the abundance of particular cell types influences group comparisons of cable allocation and crossing frequency. Such measurements complement connection-based analyses, but their interpretation depends on reconstruction quality, coordinate conventions, and the grouping of cells [8].

Three aspects of left–right organization should be distinguished. First, similar numbers of somata on the two sides describe numerical balance. Second, the fraction of an individual neuron's cable on either side describes spatial allocation. Third, the number of skeleton edges intersecting a reference plane describes repeated geometric passage across that plane. A neuron may allocate substantial cable to both sides after only one crossing, whereas a largely unilateral arbor may contain several short excursions. None of these measurements alone establishes lateralized neural activity or behavior.

We retained four annotation labels from male-cns:v1.0 [7]: male-specific (MS), sexually dimorphic (SD), potentially sexually dimorphic (pSD), and potentially male-specific (pMS). The four annotation groups differ in their cell-type composition and in the anatomical superclasses they contain. A group dominated by numerous copies of a few unilateral types can appear more unilateral than a group containing fewer neurons per type. Moreover, "potentially" annotated categories express uncertainty in the source annotation; they are not intermediate developmental states or independently validated biological classes. Comparisons should therefore preserve these labels and examine the consequences of weighting neurons or types equally.

Using the male-cns:v1.0 reconstruction of one adult male *Drosophila melanogaster*, we asked three questions. First, how do the fraction of cable on the side opposite the soma and the number of reference-plane crossings vary among the four source annotation groups? Second, which cell types account for the observed group differences, and which differences persist when each type receives equal weight or when the comparison is restricted to the central brain? Third, which named types retain similar cable-allocation measurements across changes in reference-plane position and skeleton-quality restrictions, making them candidates for cross-specimen or circuit-level studies?

2. Materials and Methods

2.1. Data Source, Selection, and Scope

This study reanalyzed public male-cns:v1.0 data associated with Berg et al. [7]. The source specimen (Z0720-07m) was a male *Drosophila melanogaster* dissected five days after

eclosion [7]. This fruit fly develops from an egg through three larval instars and a pupal stage before emerging as an adult. During metamorphosis, many larval neurons remodel their arbors as adult circuits form [9]. The reconstruction therefore captures the CNS after this developmental transition. Because structural plasticity can persist in the adult brain [10], we interpret cable allocation and crossing counts as measurements at the time of fixation. A single reconstruction cannot establish how these measurements change with adult age. The official release provides annotations and centerline skeletons in male CNS electron-microscopy coordinates [11]. The analyzed annotation snapshot contained 5933 unique body identifiers selected by a nonempty fruDsx field, a nonempty dimorphism field, or both. The selection record identifies body-annotations-male-cns-v1.0-minconf-0.5.feather as the source annotation file. All 5933 corresponding SWC files were available, and their identifiers were matched one-to-one to the annotation snapshot. File-level SHA-256 hashes defining the exact analyzed inputs are available upon reasonable request.

The four dimorphism labels defined the comparison set: male-specific (MS; $n = 1258$), sexually dimorphic (SD; $n = 771$), potentially sexually dimorphic (pSD; $n = 177$), and potentially male-specific (pMS; $n = 162$). The remaining 3565 neurons had a fruDsx annotation but no dimorphism label; they contributed to the selected-data inventory and reference-plane estimate but were not treated as a non-dimorphic control group. We grouped neurons by the dimorphism label recorded in male-cns:v1.0. For brain neurons, Berg et al. compared cell types across male and female connectomes using morphology and connectivity. A type was labeled MS when it could be identified on both sides of the male brain but had no probable female counterpart. A type was labeled SD when male and female neurons could be matched to a common developmental origin but showed consistent differences in morphology, cell number, or both. The source project used pSD when the evidence for sexual dimorphism was less certain and pMS when the evidence for male specificity was less certain. Most ventral nerve cord assignments drew on prior anatomical studies because a fully annotated female nerve cord was unavailable for the source comparison. We retained the MS, SD, pSD, and pMS labels assigned by the source study [7]. The source also assigned putative fru/dsx expression by comparing reconstructed neurons with registered light-microscopy images of labeled cells and by considering published expression evidence where available. High and low indicate confidence in the assignment. We did not assay gene expression in this specimen. All observations came from one reconstructed male CNS, with no additional animals or female skeleton measurements. Table 1 summarizes the criteria used by the source study to assign the four dimorphism labels and the separate fruDsx annotation [7].

Table 1. Operational definitions and evidence underlying the source annotations used in this study.

Source Field and Category	Operational Definition	Basis for Assignment in the Source Study
dimorphism—Male-specific (MS)	A type identified on both sides of the male nervous system for which the source study found no convincing female counterpart.	For brain types, the source compared morphology and connectivity across hemispheres and connectomes. Candidate female counterparts were evaluated against alternative type matches.
dimorphism—Sexually dimorphic (SD)	A corresponding type identified in both sexes, with a shared developmental origin and consistent sex-related differences in arbor morphology, cell number, or both.	Cross-sex type matching established the correspondence. Comparisons across hemispheres helped assess whether the observed differences were consistent.

Table 1. *Cont.*

Source Field and Category	Operational Definition	Basis for Assignment in the Source Study
dimorphism—Potentially sexually dimorphic (pSD)	A type provisionally assigned to the SD category.	The available comparative evidence suggested a sex-related difference, and the source assigned lower confidence to that interpretation.
dimorphism—Potentially male-specific (pMS)	A type provisionally assigned to the MS category.	The available matching evidence suggested male specificity, but uncertainty remained as to whether a female counterpart could be identified.
fruDsx—Putative *fruitless* and/or *doublesex* expression	A separate annotation indicating putative *fru* expression, *dsx* expression, or coexpression.	The source compared reconstructed neurons with registered light-microscopy images of genetically labeled cells and considered published expression evidence where available. High and low indicate confidence in the assignment.

Definitions follow Berg et al. [7]. Direct cross-connectome comparisons were most extensive for brain types. Most ventral nerve cord dimorphism assignments relied on published anatomical studies because the source study lacked a fully annotated female ventral nerve cord for comparison. A missing fruDsx entry indicates that no assignment was recorded. Gene expression was not measured in the present specimen.

Table 2 shows the overlap between the four dimorphism labels and the source fruDsx annotations. All 2368 neurons with a dimorphism label were included, irrespective of soma-side eligibility.

Table 2. Overlap between dimorphism labels and fruDsx annotations in male-cns:v1.0.

Dimorphism Group	Total *n*	*fru* Only, H/L	*dsx* Only, H/L	Coexpression, H/L	Any fruDsx Annotation, *n* (%)	No Annotation, *n* (%)
MS	1258	720/29	118/10	128/31	1036 (82.4)	222 (17.6)
SD	771	217/49	10/0	4/2	282 (36.6)	489 (63.4)
pSD	177	16/16	4/0	0/0	36 (20.3)	141 (79.7)
pMS	162	44/2	6/0	22/19	93 (57.4)	69 (42.6)

H and L denote high and low confidence in the source annotation, respectively. The three annotated categories are mutually exclusive. "Any fruDsx annotation" is their sum. Percentages use the full number of neurons in each row. "No annotation" indicates that no call was recorded in the source dataset. Gene expression in those neurons remains unknown.

2.2. Skeleton Geometry and Quality Checks

SWC coordinates were converted to micrometers using 0.008 µm per coordinate unit, following the official data specification [11]. Each node–parent pair defined a straight three-dimensional segment, and cable length was the sum of Euclidean segment lengths. Coordinates, edges, and all disconnected components were retained without additional smoothing, pruning, resampling, or artificial reconnection. SWC radii were not used to estimate neurite diameter or volume. Increasing × corresponds to the left side according to the soma annotations in this snapshot.

The coordinate unit is not the geometric resolution of the skeleton. The supplied headers identify 5687 files with downresLevel = "coarse" and 246 files with numeric settings (0, 1, or 2). The recorded downsampling intervals also vary. Accordingly, all reported lengths and intersections refer to source-resolution centerlines, not full-resolution membrane reconstructions. The source settings are retained in the measurement tables. Checks required unique node identifiers, existing parents, positive finite total length, and conservation of cable length during splitting. All parent identifiers preceded their children, ruling out

cycles in these files. Multiple roots were recorded as disconnected components rather than interpreted as additional neurons.

2.3. Operational Reference Plane and Cable Allocation

An operational left–right reference plane was estimated from all selected neurons with both a left/right somaSide annotation and a recorded somaLocation. The median soma × coordinates were 61,405 units for left-labeled somata ($n = 2719$) and 36,008 units for right-labeled somata ($n = 2693$). Their midpoint was $x_0 = 48{,}706.5$ units, or 389.652 µm. This single plane is a reproducible coordinate partition, not an independently registered anatomical midline surface. Soma-side agreement and plane-displacement analyses were used to assess its limitations.

Each segment crossing x_0 was split at its exact linear intersection with the plane. The lengths on $x > x_0$ and $x < x_0$ were accumulated as L and R, respectively. A segment lying entirely in the plane would contribute half its length to each side; none occurred at the reference plane. Total cable length was $T = L + R$, and the signed laterality index was $LI = (R - L)/T$. Its magnitude, $|LI|$, ranges from zero for equal cable allocation to one for exclusively unilateral cable.

Contralateral cable fraction was defined relative to the source somaSide annotation: $C = R/T$ for left-labeled neurons and $C = L/T$ for right-labeled neurons. Neurons labeled midline (M) or lacking somaSide were excluded from analyses of C and cable-allocation class without substituting root position for soma side. This excluded one SD neuron and 14 pSD neurons, leaving $n = 2353$. All 2368 neurons remained eligible for total length, $|LI|$, and crossing counts. Because $|LI| = |1 - 2C|$ wherever C is defined, these are related descriptions rather than independent endpoints.

Continuous contralateral cable fraction (C) was the primary measure of cable allocation. For the secondary summary, we classified neurons as ipsilateral-dominant when $C < 0.05$, bilateral when $0.05 \leq C \leq 0.95$, and contralateral-dominant when $C > 0.95$. The symmetric 5% tolerance allowed an arbor with more than 95% of its reconstructed cable on one side of the reference plane to be classified as predominantly unilateral even when some cable extended to the opposite side. We retained 5% as the reporting convention used in the original analysis and repeated the classification at 2.5% and 10% to assess the effect of halving and doubling this tolerance. These cutoffs serve a descriptive purpose and have no independently established biological boundary. The SWC centerlines describe cable geometry but cannot identify axonal outputs, locate synaptic partners, or establish the direction of information transfer.

We counted a reference-plane crossing whenever the endpoints of a reconstructed segment lay strictly on opposite sides of x_0. This count measures geometric intersections with the plane. For disconnected skeletons, we counted crossings only along reconstructed segments and made no assumptions about the paths connecting separate components.

2.4. Descriptive Statistics and Cell-Type Comparisons

Continuous measurements are summarized by medians and interquartile ranges; all quantiles use linear interpolation. Neuron-level distributional differences were described using Kruskal–Wallis H and $\varepsilon^2 = (H - k + 1)/(N - k)$, with $k = 4$ groups. The association between source annotation group and cable-allocation class was summarized by Pearson's χ^2 and Cramér's V. Because the contralateral-dominant class was rare, its contingency-table reference probability was estimated from 100,000 fixed-margin random tables, using $(b + 1)/(B + 1)$, where b is the number of simulated statistics at least as large as observed. These reference calculations assume exchangeable neurons and are exploratory descriptors within this reconstruction; they cannot supply between-animal replication [12].

To assess cell abundance, each annotated cell type was represented by its median measurement, and type medians were averaged with equal weight within each group. For crossing counts, the same type medians were also averaged with weights proportional to neuron count to isolate the effect of weighting. To quantify the influence of TmY21 on the SD cable-allocation summary, we recalculated the proportion of ipsilateral-dominant SD neurons after omitting this type. To identify the types contributing most to the equally weighted SD crossing summary, we ranked SD types by their median crossing count and calculated the proportion of the sum of all SD type medians contributed by the five highest-ranked types. Each type contributed one median to a single annotation group. Six neurons had no assigned cell type and therefore could not be included in a type-specific median. We also excluded 12 neurons from two types, ANXXX116 and SMP726m, because the dimorphism label varied among neurons within each type. Consequently, neither type's median could be assigned unambiguously to one group.

The resulting 2350 neurons represented 476 types: 265 MS, 102 SD, 64 pSD, and 45 pMS. A type with no eligible soma-side measurement was omitted only from the C comparison. Each group was resampled independently at the type level, with replacement, to obtain 10,000 bootstrap differences from the MS reference. The 2.5th and 97.5th percentiles define pointwise 95% intervals conditional on the observed type collection. These intervals describe sensitivity to the representation of types, not uncertainty across flies.

Superclass composition was tabulated explicitly. Type-level comparisons were repeated for central-brain intrinsic neurons (source superclass cb_intrinsic). Within this superclass, exploratory ordinary least-squares (OLS) models used either C or $\log(1 + \text{crossing count})$ as the outcome, MS as the group reference, and standardized log cable length, its square, log root count, source tracing status, and source downresLevel as covariates. Standard errors used a cell-type-clustered sandwich covariance with the finite-sample factor $G/(G-1) \times (N-1)/(N-p)$, where G is the number of clusters and p the number of model terms; intervals used a t reference with $G-1$ degrees of freedom. Six group coefficients across the two outcomes were adjusted together using the Holm procedure. In the central-brain regression models, each neuron was an observation with its own dimorphism label. The cell-type identifier defined the cluster for estimating standard errors. Eligible neurons from a mixed-label type therefore shared a cluster while retaining their individual labels. Neurons without a type identifier were excluded because their cluster membership was unknown. We used OLS for C because each group coefficient gives an adjusted difference in mean C on its original scale. Because C is bounded between 0 and 1 and can take either endpoint, we examined the OLS fitted values, residual variance, and leverage. We also refitted each OLS model after omitting one cell type at a time to assess the influence of individual types on the group contrasts. For C, we fitted a fractional-logit model to the same neurons using the same covariates and cell-type-clustered covariance. This model accommodates exact zeros and ones and constrains the fitted mean to the unit interval [13]. To compare its results directly with OLS, we averaged the fitted differences between each group and MS over the observed covariate distribution. All adjusted contrasts were exploratory and conditional on this specimen.

2.5. Sensitivity, Visualization, and Reproducibility

All geometric measurements were recomputed after displacing the reference plane by −5, −2, −1, +1, +2, or +5 μm along x. Rank correlations and agreement in cable-allocation class were compared with the reference measurements. Thresholds for cable-allocation classes of 0.025 and 0.10 were evaluated in addition to 0.05. Further summaries restricted the data to single-root skeletons, to files labeled "coarse", or to neurons without a disagreement between annotated soma side and recorded soma x position. These checks

assess computational sensitivity; they do not validate a curved anatomical midline or reconstruct missing branches.

Illustrative neurons were selected deterministically within each group from those with known soma side. For cable length, C, and crossing count, average-tie percentile ranks were calculated; the neuron minimizing the sum of squared distances from rank 0.5 was selected, with body identifier resolving ties. All edges were plotted in an x–y projection using common axes, without geometry simplification. Selection was based on cable length, contralateral cable fraction (C), and reference-plane crossing count. Similarity to other neurons in the group in overall arbor shape was not assessed. Analysis used Python 3.12.14, NumPy 2.3.5, pandas 2.2.3, and SciPy 1.17.0 [14], with random seed 20261002. Exact edge-splitting cases, reflected geometries, and dataset-wide identities were checked using a verification script available upon reasonable request.

During revision, we screened cell types for stability of the median contralateral cable fraction (C). An eligible type had to carry a consistent dimorphism label, belong to one anatomical superclass, and include at least two neurons with left-sided somata and two with right-sided somata. Where soma coordinates were available, the recorded position had to agree with the annotated side. We retained types whose median C changed by no more than 0.02 from baseline at every tested reference-plane displacement. We also repeated the calculation separately for single-root skeletons and for skeletons recorded at the coarse setting. Each subset had to retain at least half of the neurons in the type, include both soma sides, and yield a median C within 0.02 of baseline. We used this two-percentage-point tolerance as an operational criterion for follow-up. Crossing counts were recorded separately.

3. Results

3.1. Analyzed Neurons and Reconstruction Properties

The 5933 source skeletons contained 17,837,843 nodes, and all had valid positive cable lengths. Of the 2368 comparison neurons, 403 had more than one root: 237 MS, 114 SD, 32 pSD, and 20 pMS neurons. The respective numbers recorded with the coarse skeleton setting were 1225, 694, 175, and 160. These properties were retained in the tables and incorporated into sensitivity analyses. Source soma counts were close to balanced between left and right within each group (Table 3); this numerical balance does not imply symmetry of individual arbors. Deterministically selected examples illustrate both predominantly unilateral and cross-plane geometries (Figure 1).

Table 3. Neuron-level morphology and annotated soma side in the four sex-associated groups.

Group	Total *n*	Eligible for C, *n*	Excluded from C, *n*	Soma L/R	Cable Length (µm)	Absolute LI	Crossing Count
MS	1258	1258	0	635/623	2512 (1919–3227)	0.758 (0.630–1.000)	1.00 (0.00–2.00)
SD	771	770	1	381/389	1435 (957–2666)	1.000 (0.839–1.000)	0.00 (0.00–1.00)
pSD	177	163	14	81/82	2959 (1964–5929)	0.675 (0.261–0.972)	4.00 (1.00–13.00)
pMS	162	162	0	81/81	3186 (2320–4891)	0.600 (0.363–0.767)	4.00 (1.00–13.75)

Values are medians (interquartile ranges), except for neuron counts. Total *n* is the denominator for cable length, absolute laterality index (LI), and crossing count. Eligible *n* is the denominator for contralateral cable fraction (C) and cable-allocation class. One SD neuron and 14 pSD neurons had a midline or missing soma-side annotation, leaving 2353 of 2368 neurons eligible for soma-relative measurements. L/R indicates the numbers of left- and right-labeled somata.

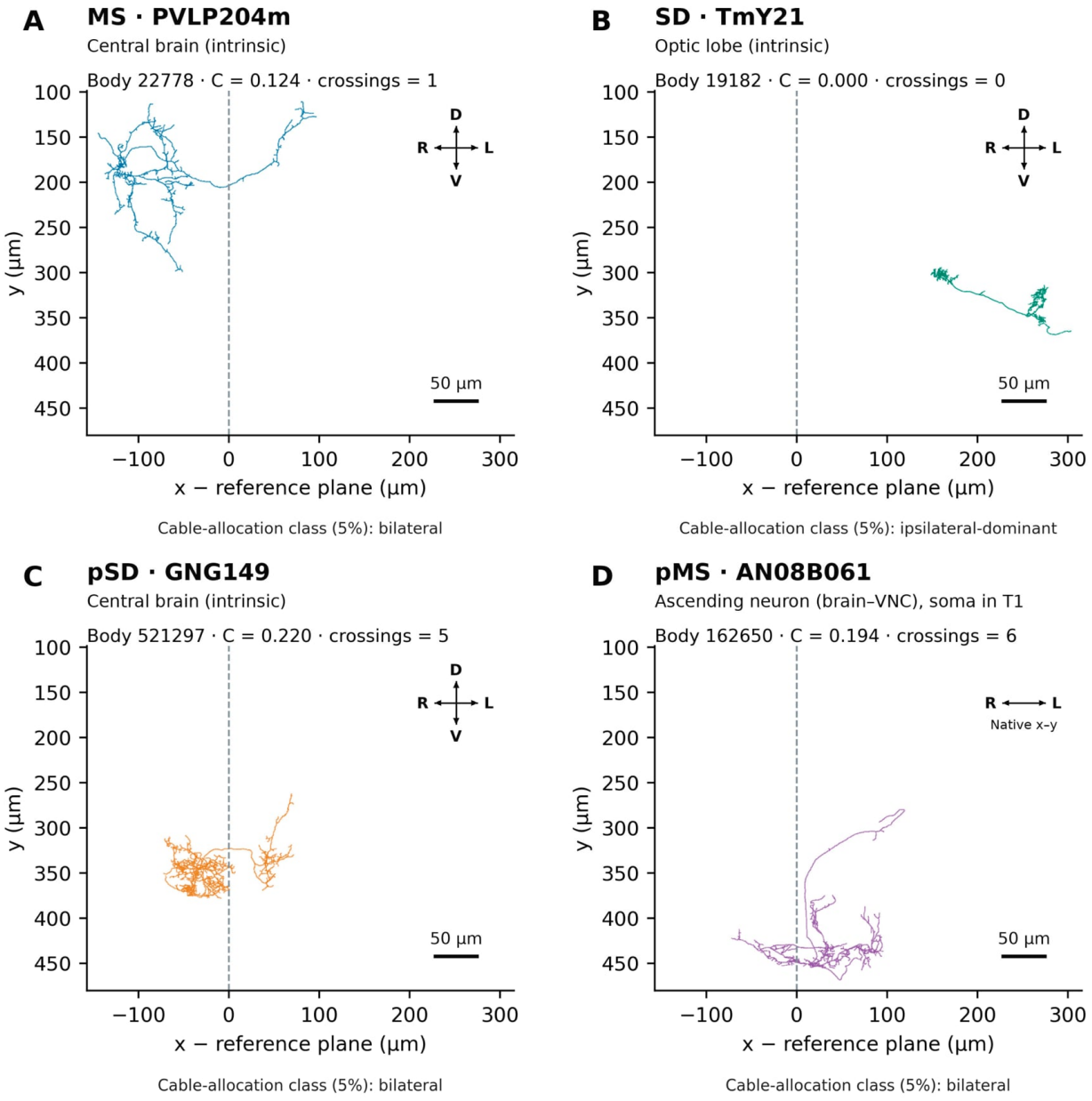


Figure 1. Cable allocation and reference-plane crossings in four individual neurons. (**A**) PVLP204m (MS, body 22778), a central-brain intrinsic neuron. (**B**) TmY21 (SD, body 19182), an optic-lobe intrinsic neuron. (**C**) GNG149 (pSD, body 521297), a central-brain intrinsic neuron. (**D**) AN08B061 (pMS, body 162650), an ascending neuron with its soma in the prothoracic neuromere (T1). Within each annotation group, one neuron was selected for its proximity to the median ranks of cable length, contralateral cable fraction (**C**), and crossing count. The examples illustrate these measurements in individual reconstructions. The selection criterion did not assess whether an arbor shape was typical of its group. All panels show native x–y projections at the same spatial scale. R and L indicate the specimen's right and left. In panels A–C, D and V indicate the approximate dorsal and ventral directions of the brain. Panel D shows only right and left because the projection collapses the brain–ventral nerve cord extent along z. Each scale bar represents 50 µm. The dashed line marks the reference plane at x_0 = 389.652 µm. Cable fractions and crossings were calculated in three dimensions. Line width does not indicate neurite caliber. Source geometry from male-cns:v1.0 [7,11], licensed under CC BY 4.0.

3.2. Continuous Cable Allocation and Secondary Cable-Allocation Classes

Median contralateral cable fraction was 0.128 in MS, 0.000 in SD, 0.190 in pSD, and 0.206 in pMS neurons (Figure 2A). Median cable length ranged from 1435 µm in SD neurons

to 3186 μm in pMS neurons. The SD group had a median absolute laterality index of 1.000 (Table 3). The neuron-level Kruskal–Wallis summaries were H = 338.84 and $\varepsilon^2 = 0.142$ for cable length, H = 397.11 and $\varepsilon^2 = 0.167$ for |LI|, and H = 396.55 and $\varepsilon^2 = 0.168$ for C. These summarize separation among the recorded neurons, subject to the dependence between cells and between |LI| and C.

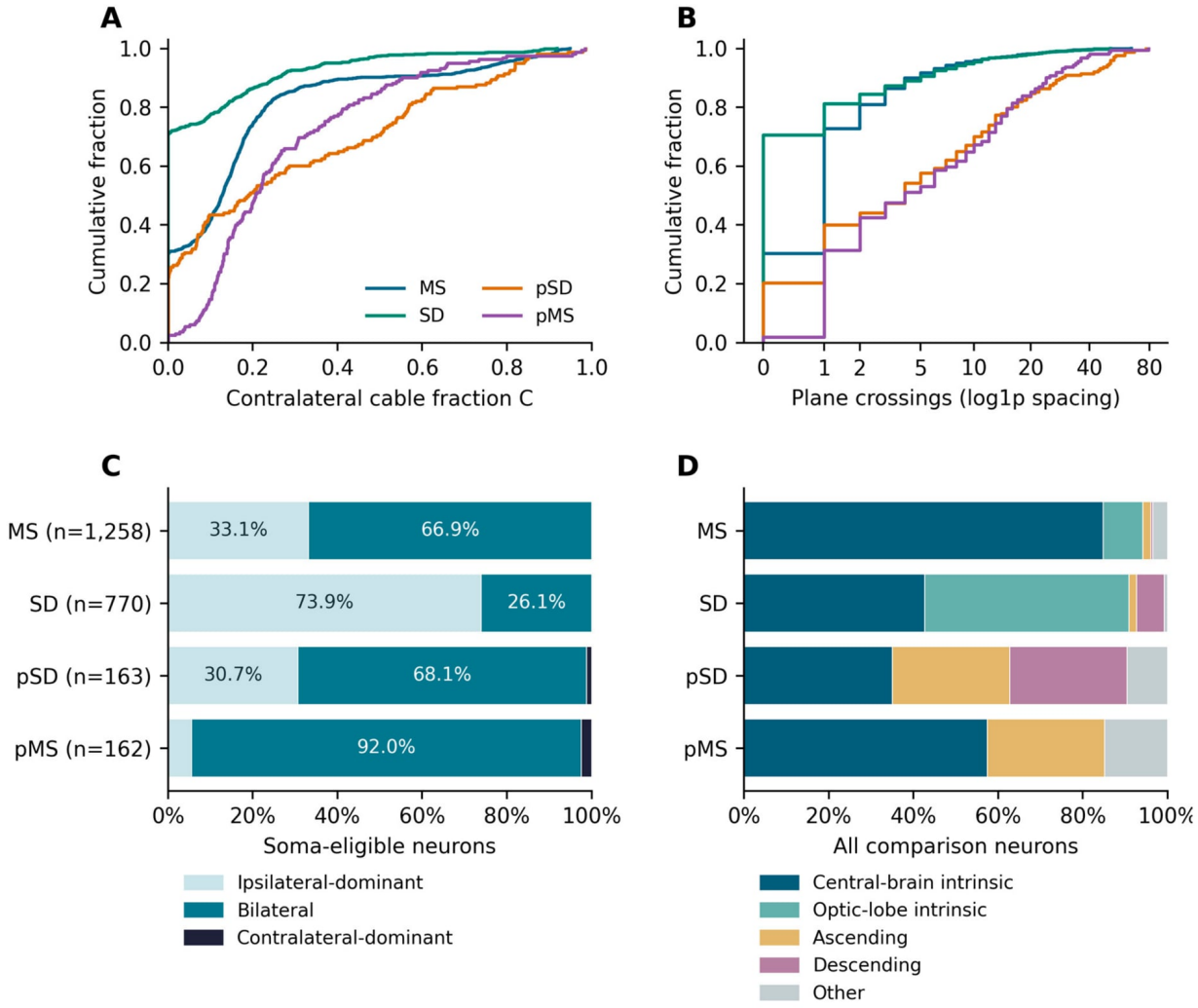


Figure 2. Neuron-weighted morphology and group composition. (**A**) Empirical cumulative distributions of contralateral cable fraction (**C**); the four sample sizes are 1258, 770, 163, and 162. (**B**) Cumulative distributions of plane-crossing edges, with log(1 + count) spacing and ticks labeled in the original count units; all 2368 neurons are included. (**C**) Percentages of soma-eligible neurons in each cable-allocation class. (**D**) Anatomical superclass composition among all neurons in each annotation group. MS, male-specific; SD, sexually dimorphic; pSD, potentially sexually dimorphic; pMS, potentially male-specific. No independent-animal error bars are implied.

As a secondary summary, we classified neurons by their contralateral cable fraction using the 5% threshold (Table 4 and Figure 2C). Among SD neurons with an unambiguous soma-side annotation, 569 of 770 (73.9%) had ipsilateral-dominant cable allocation. Bilateral cable allocation was observed in 841 of 1258 MS neurons (66.9%), 111 of 163 pSD neurons (68.1%), and 149 of 162 pMS neurons (92.0%). Across all four groups, six neurons met the contralateral-dominant threshold. The association between source annotation group and cable-allocation class was summarized by Pearson's $\chi^2 = 484.18$ and Cramér's V = 0.321. These statistics describe the neurons observed in this single specimen.

Table 4. Cable-allocation classes among neurons with an unambiguous soma-side annotation.

Group	Eligible *n*	Ipsilateral-Dominant	Bilateral	Contralateral-Dominant
MS	1258	417 (33.1%)	841 (66.9%)	0 (0.0%)
SD	770	569 (73.9%)	201 (26.1%)	0 (0.0%)
pSD	163	50 (30.7%)	111 (68.1%)	2 (1.2%)
pMS	162	9 (5.6%)	149 (92.0%)	4 (2.5%)

Neurons were classified as ipsilateral-dominant when $C < 0.05$, bilateral when $0.05 \leq C \leq 0.95$, and contralateral-dominant when $C > 0.95$. Percentages use the soma-eligible counts in Table 3. The same 15 neurons were excluded from summaries of C and cable-allocation class.

3.3. Crossing Counts and Anatomical Composition

Median crossing counts were 1 in MS, 0 in SD, and 4 in both potentially annotated groups (Table 3; Figure 2B). At least one crossing was present in 69.7%, 29.4%, 79.7%, and 98.1%, respectively. The neuron-level distributional summary was $H = 446.93$ and $\varepsilon^2 = 0.188$. These differences coincided with substantial variation in anatomical composition: central-brain intrinsic neurons represented 1067/1258 MS neurons (84.8%) but 329/771 SD neurons (42.7%), while optic-lobe intrinsic neurons accounted for 372/771 SD neurons (48.2%). Ascending and descending neurons together accounted for 98/177 pSD neurons (55.4%; Figure 2D).

All 372 optic-lobe intrinsic SD neurons belonged to TmY21. Each had a contralateral cable fraction of zero and no reference-plane crossings. This single type accounted for 372 of the 569 ipsilateral-dominant SD neurons (65.4%). After TmY21 was omitted, 197 of the remaining 398 soma-eligible SD neurons (49.5%) were ipsilateral-dominant, compared with 569 of 770 (73.9%) in the full group. Five SD types had particularly high median crossing counts: dMS9 (37), GNG005 (36), DNp68 (34.5), DNp13 (32.5), and ANXXX013 (26.5). Together, these types contained nine neurons and contributed 166.5 of the 513 summed SD type-median crossings (32.5%).

3.4. Equal Type Weighting and Central-Brain Analyses

Equal type weighting changed the interpretation of crossing counts. The mean of type-median counts was 3.22 for MS and 5.03 for SD, giving an SD − MS difference of +1.81 crossings (pointwise 95% type-bootstrap interval, 0.12 to 3.66). Thus, the lower neuron-level median in SD did not translate into a lower average of type medians. Holding the type-median statistic fixed, weighting by neuron count instead gave 2.06 for MS and 1.72 for SD; equal weighting therefore reversed this ordering as well. For C, the corresponding means were 0.190 for MS and 0.140 for SD, with a difference of −0.050 (−0.094 to −0.003). The pSD − MS and pMS − MS differences in C were +0.110 and +0.110, respectively (Figure 3A,B).

Within central-brain intrinsic types, the SD − MS difference in mean type-median C was −0.069 (−0.110 to −0.026), whereas the crossing difference was +0.80 (−0.40 to 2.24). The pSD − MS and pMS − MS C differences were −0.052 (−0.120 to 0.024) and +0.015 (−0.034 to 0.070), respectively. The larger positive C differences in the pooled potentially annotated groups therefore did not persist within this superclass (Figure 3C,D). The type counts eligible for central-brain C comparisons were 233 MS, 73 SD, 17 pSD, and 22 pMS. The SD–MS difference in mean type-median contralateral cable fraction was negative both across all eligible types (−0.050) and within central-brain intrinsic types (−0.069). In the optic lobe, TmY21 (SD, 372 neurons) and Tm26 (MS, 103 neurons) both had zero contralateral cable and zero crossings in every recorded neuron. For crossing counts, the equally weighted SD–MS difference decreased from +1.81 across all types to +0.80 within the central brain, where the type-resampling interval included zero.

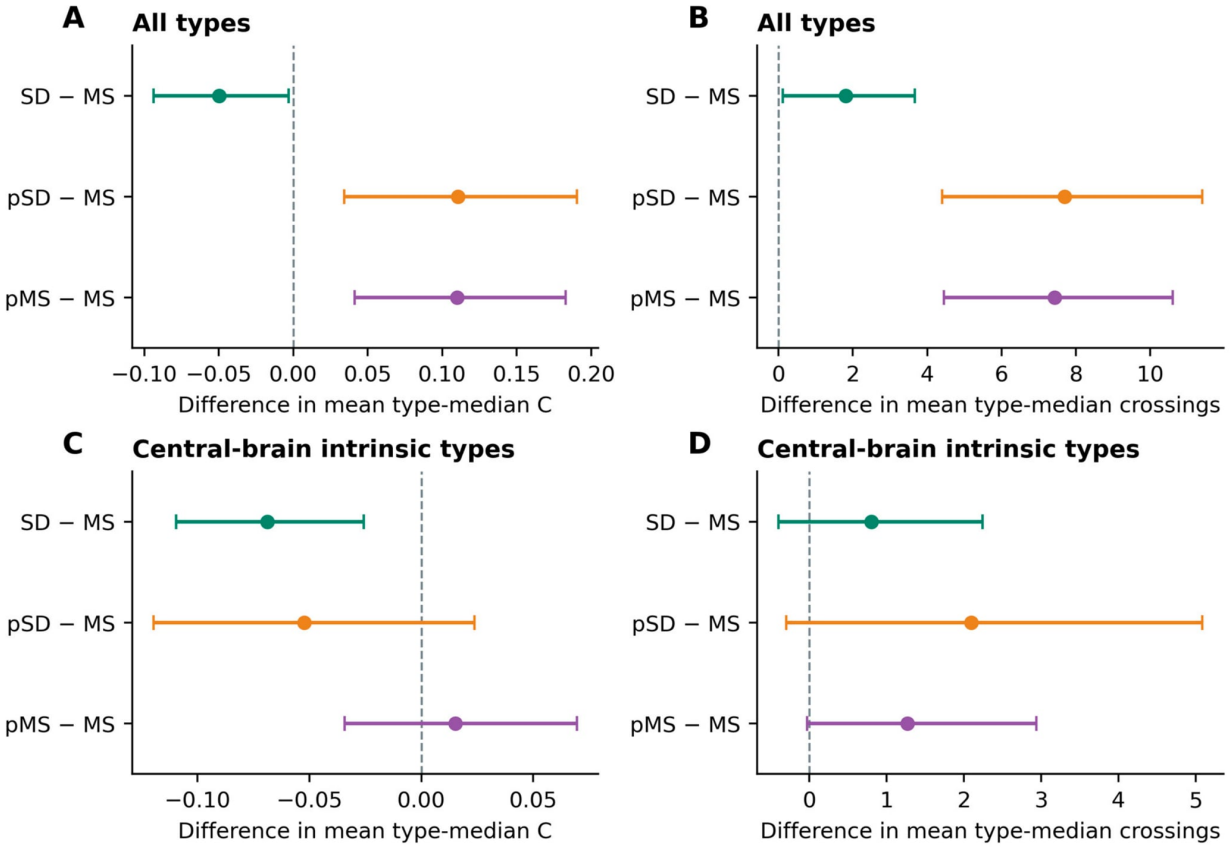


Figure 3. Differences after giving each cell type equal weight. Points show differences from MS in the mean of within-type medians; bars are pointwise 95th percentile intervals from 10,000 type-level bootstrap samples. (**A**,**B**) All eligible types; (**C**,**D**) central-brain intrinsic types. Left panels summarize contralateral cable fraction (**C**); right panels summarize crossing counts. Positive values indicate larger measurements than MS. The zero reference is dashed. For all-type C comparisons, $n = 265$, 101, 58, and 45 types; for all-type crossing comparisons, $n = 265$, 102, 64, and 45. Central-brain C counts are 233, 73, 17, and 22; crossing counts are 233, 74, 19, and 22. Intervals concern the observed type collection within one CNS, and are not simultaneous intervals or estimates of between-fly variability.

The exploratory OLS model for C included 1,540 central-brain intrinsic neurons in 346 cell-type clusters (Table 5). Of these neurons, 451 (29.3%) had C = 0. The model explained little of the observed variation ($R^2 = 0.057$), residual variance was nonconstant, and three fitted values fell below zero (minimum −0.021). Using MS as the reference, the adjusted mean differences in C were −0.078 for SD, −0.094 for pSD, and −0.018 for pMS. The corresponding standardized differences from the fractional-logit model were −0.077, −0.096, and −0.019. All three OLS contrasts for C remained negative when cell types were omitted one at a time.

The exploratory model for log(1 + crossing count) included 1545 neurons in 349 cell-type clusters ($R^2 = 0.087$). The pMS − MS coefficient was +0.366 (pointwise 95% cluster interval, +0.141 to +0.590). The pSD − MS coefficient was sensitive to the inclusion of individual types, ranging from −0.143 to +0.043 when one type was omitted at a time. Maximum leverage was approximately 0.50 in both OLS models. These contrasts describe adjusted differences among neurons in this specimen. The intervals do not quantify variation across animals.

Table 5. Exploratory adjusted contrasts within central-brain intrinsic neurons.

Outcome	Contrast	Coefficient	95% Cluster Interval	Holm p
C	SD − MS	−0.078	−0.142 to −0.014	0.066
C	pSD − MS	−0.094	−0.163 to −0.025	0.040
C	pMS − MS	−0.018	−0.070 to 0.034	0.990
log(1 + crossings)	SD − MS	−0.197	−0.388 to −0.005	0.131
log(1 + crossings)	pSD − MS	−0.059	−0.442 to 0.324	0.990
log(1 + crossings)	pMS − MS	0.366	0.141 to 0.590	0.009

Models include log cable length and its square, log root count, tracing status, and skeleton downresLevel. C: 1540 neurons in 346 type clusters; log(1 + crossings): 1545 neurons in 349 clusters. Intervals are pointwise and use type-clustered standard errors; p values are Holm-adjusted across all six displayed contrasts. These reference probabilities and intervals do not represent biological replication across animals.

3.5. Sensitivity to Geometric and Reconstruction Choices

At reference-plane displacements of ±2 µm, 99.49–99.75% of eligible neurons retained their baseline cable-allocation class. At −5 and +5 µm, respectively, 18 and 22 of the same 2353 neurons changed class, corresponding to 99.24% and 99.07% agreement with baseline. At these two displacements, the rank correlations between baseline and shifted crossing counts ranged from 0.944 to 0.957. With the reference plane held fixed, Cramér's V for the association between annotation group and cable-allocation class was 0.322 at the 2.5% tolerance, 0.321 at 5%, and 0.273 at 10%. Increasing the tolerance from 5% to 10% reassigned 8.3% of the 2353 eligible neurons to a different class. The underlying C values were unchanged, illustrating why we use continuous C for anatomical comparisons and the classes for descriptive summaries.

Recorded soma x positions disagreed with the annotated side for 115/5412 neurons used to assess the plane; 33 disagreements were within 2 µm of it. Among the four comparison groups, 79 neurons showed a disagreement. All 79 neurons were retained in the primary analysis. In a separate sensitivity analysis excluding them, median C changed from 0.128 to 0.123 in MS, remained 0.000 in SD, changed from 0.190 to 0.160 in pSD, and changed from 0.206 to 0.199 in pMS. Restriction to single-root skeletons retained 1965 neurons and yielded median crossing counts of 1, 0, 4, and 5.5. Restriction to the coarse setting retained 2254 neurons, with median counts of 1, 0, 4, and 4. These checks preserved broad neuron-level patterns, while highlighting the limits of a global plane and incomplete centerline reconstruction.

3.6. Candidate Cell Types for Follow-Up Studies

Of the 476 types with a consistent dimorphism label, 139 met the criteria for stable median C, comprising 95 MS, 28 SD, 5 pSD, and 11 pMS types. Table 6 presents nine examples selected to illustrate different anatomical regions, cable allocations, and follow-up questions. AOTU008 and mAL_m8 provide a comparison in which median crossing count is the same but median C differs substantially. INXXX062 illustrates a different case. Its median C changed by less than 0.01 across plane positions, while its median crossing count ranged from 23 to 27.

Among the candidates in Table 6, AOTU008 belongs to the previously described aSP-i population [7]. Both AOTU008 and mAL_m8 carry high-confidence *fru* annotations in the source dataset. Two further candidates, pC1_16b and pC1_13b, link the inventory to the *dsx*-associated pC1 cluster described by Rideout et al. [3]. The source assigns pC1_16b a high-confidence annotation for fru/dsx coexpression and pC1_13b a high-confidence *dsx* annotation [7]. The latter retains its pMS label. These records identify candidate subtypes for cell-specific expression studies.

Table 6. Selected cell types with stable contralateral cable allocation and proposed follow-up analyses.

Cell Type	Source Label	Anatomical Group	*n*	Median C	Maximum Change in Median C	Median Crossings at Baseline (Range Across Shifts)	Proposed Follow-up
TmY21	SD	Optic-lobe intrinsic	372	0.000	0.0000	0 (0–0)	Compare cable allocation with that of the matched female visual type.
Tm26	MS	Optic-lobe intrinsic	103	0.000	0.0000	0 (0–0)	Reassess possible female homologs using morphology and synaptic partners.
AOTU008	SD	Central-brain intrinsic	25	0.120	0.0034	1 (1–1)	Compare the distribution of synaptic inputs and outputs with that of mAL_m8.
mAL_m8	MS	Central-brain intrinsic	16	0.851	0.0027	1 (1–1)	Determine whether the extensive opposite-side arbor carries predominantly inputs, outputs, or both.
pC1_16b	MS	Central-brain intrinsic	8	0.197	0.0085	2 (2–3)	Record responses to left- and right-sided stimulation after verifying cell-type identity.
pC1_13b	pMS	Central-brain intrinsic	4	0.128	0.0018	1 (1–1)	Assess possible female pC1 counterparts before comparing arbor geometry across sexes.
AVLP297	pSD	Central-brain intrinsic	8	0.000	0.0000	0 (0–0)	Test whether a matched female type also has exclusively soma-side cable.
DNge116	pSD	Descending	4	0.547	0.0002	1 (1–1)	Map presynaptic sites on each side of the ventral nerve cord.
INXXX062	pMS	Ventral nerve cord intrinsic	4	0.283	0.0094	27 (23–27)	Reassess individual crossings after registration to a local anatomical midline.

C is the fraction of reconstructed cable on the side of the reference plane opposite the annotated soma. Maximum change is the largest absolute difference between the type-median C at baseline and after a plane displacement of ±1, ±2, or ±5 µm. Crossing ranges describe variation in the type median across plane positions. Soma coordinates were available for 366 of 372 TmY21 neurons, 100 of 103 Tm26 neurons, and all neurons in the other seven types. The proposed follow-up analyses are prospective. Stability was assessed within the reconstructed male specimen. For types labeled MS or pMS, a matched cross-sex comparison first requires assessing whether a corresponding female type can be identified.

4. Discussion

This analysis separates soma–number balance, reconstructed cable allocation, and repeated plane crossings in sex-associated neurons of one male fly. The strongest neuron-weighted pattern was the high proportion of SD neurons with ipsilateral-dominant cable allocation, contrasted with frequent bilateral allocation in the pMS group. The accompanying measurements provide an explicit geometric description of these annotation groups, without converting source sex-association labels into evidence of new male–female differences.

The high proportion of ipsilateral-dominant neurons in the SD group was largely attributable to one abundant optic-lobe type, TmY21. Once this type was set aside, approximately half of the remaining SD neurons were ipsilateral-dominant. The opposite influence was evident for crossing counts: several sparsely represented SD types crossed the plane repeatedly and made a substantial contribution when each type received equal weight. The weighting reversal therefore reflects the coexistence of distinct arbor geometries within the same source annotation group. Within the central brain, SD types still had a lower mean type-median contralateral cable fraction than MS types, although the difference in crossing counts was less clearly resolved.

The potentially annotated groups also illustrate why annotation uncertainty and anatomy should be kept separate. Their larger pooled contralateral fractions were substantially attenuated, or changed direction, in central-brain comparisons. The adjusted pSD C coefficient was negative relative to MS, whereas the pooled type-level contrast was positive. Consequently, neither a high bilateral fraction nor a high crossing count should be used to validate a "potentially" sex-associated label. The results instead identify the anatomical strata and named types that should be examined in matched comparisons or targeted experiments.

Cable allocation and crossing count capture different geometric properties. The former measures how much reconstructed arbor lies in each coordinate half-space; the latter counts repeated intersections of individual edges. They can diverge because branches may travel far after one crossing or make several short excursions near the plane. A crossing edge is not itself a synaptic connection or evidence that information passes between functional hemispheres. Kimura et al. [2] used genetic labeling to show that the mAL neuronal cluster differs between male and female flies in both cell number and branching pattern. Rideout et al. [3] used a doublesex driver to manipulate labeled neurons and examine their contribution to female receptivity to mating. Cachero et al. [4] compared labeled fruitless neuronal lineages across sexes and mapped the brain regions in which their arbors differed.

Our measurements identify a specific question for synaptic analysis. In this male specimen, mAL_m8 and AOTU008 each had a median of one reference-plane crossing, yet their median contralateral cable fractions were 0.851 and 0.120, respectively. For each neuron, the fraction of presynaptic sites and the fraction of postsynaptic sites on the side opposite its annotated soma could be calculated separately. Comparing these fractions between the two types would test whether the greater contralateral cable allocation in mAL_m8 is accompanied by a greater contralateral share of its inputs, its outputs, or both.

Several limitations constrain interpretation. Translating the plane tests sensitivity to its position along the x-axis. Local curvature or changes in orientation between the brain and ventral nerve cord could affect individual measurements even when most neurons retain the same cable-allocation class. All neurons belong to one specimen; cell-type resampling and clustered covariance cannot replace independent flies. The selected fruDsx-or-dimorphism subset does not estimate the distribution in all CNS neurons. Source annotation criteria may themselves use anatomical information, so morphology–label associations are not independent validation of sex specificity. Morphological comparisons contributed to the source study's assignment of the dimorphism labels [7]. Our measurements therefore

describe cable geometry within those source-defined groups, but they cannot independently establish that a type is male-specific or that its morphology differs between sexes. Moving the reference plane by ±5 µm did not change which neurons were eligible for soma-relative measurements. The same 2353 neurons were analyzed at each position. One SD neuron and 14 pSD neurons had a midline or missing soma-side annotation and therefore contributed to crossing counts but had no defined C. A separate sensitivity analysis omitted 79 neurons whose recorded soma coordinates disagreed with their annotated side at the original plane. This omission preserved the ordering of the four group medians, but its effect was greatest in pSD, where median C fell from 0.190 to 0.160. The SD median remained 0.000. One possible explanation for a coordinate–annotation disagreement is that a single global plane follows the local anatomical midline less closely in some regions than in others. Excluding such neurons could therefore change the anatomical composition of a group. The restricted medians describe how sensitive the results are to that exclusion. Establishing the anatomical accuracy of the plane would require an independently registered midline.

In addition, the source skeletons have heterogeneous downsampling settings and many contain disconnected components. The single-root and coarse-only analyses assess sensitivity to two recorded features of the reconstructions. A single-root skeleton can still be incomplete, and an untraced segment may contain an unknown length of cable on either side of the plane or an unobserved crossing. Small crossings are especially dependent on skeletonization and plane placement. The regression models account for recorded proxies for these issues but cannot measure residual reconstruction error or establish causal effects of group labels. Finally, bootstrap intervals are conditional and pointwise, and multiple related measurements were explored. The appropriate contribution is a reproducible anatomical inventory and a demonstration of how weighting and composition affect interpretation, with testable candidates for future cross-specimen work.

5. Conclusions

We aimed to compare cable allocation and reference-plane crossing counts among four sex-associated annotation groups in one adult male *Drosophila melanogaster* and to assess how cell-type weighting affected the crossing-count comparison. Median contralateral cable fraction was lower in SD neurons than in MS neurons. For crossing counts, the mean of the cell-type medians was lower in SD than in MS when each type was weighted by its neuron count. Giving each type equal weight reversed this ordering. Reporting continuous cable allocation, crossing counts, type-level summaries, and reconstruction sensitivity together provides a more defensible description than a single aggregate laterality ranking. Independent specimens, matched female neurons, and anatomical midline validation are needed before extending these observations to population-level sexual dimorphism or functional lateralization.

Author Contributions: Conceptualization, D.S.; methodology, B.-K.K. and D.S.; software, D.S.; formal analysis, B.-K.K. and D.S.; investigation and data curation, B.-K.K.; visualization, D.S.; writing—original draft preparation, B.-K.K. and D.S.; writing—review and editing, B.-K.K. and D.S.; supervision, D.S. All authors have read and agreed to the published version of the manuscript.

Funding: This paper was supported by the Sehan University Research Fund in 2026.

Institutional Review Board Statement: Not applicable. This study used publicly released neuronal reconstructions and involved no new experiments on animals or humans.

Informed Consent Statement: Not applicable.

Data Availability Statement: The original male-cns:v1.0 skeletons and annotations are publicly available at https://male-cns.janelia.org/download/ (accessed on 25 November 2026) under the

Creative Commons Attribution 4.0 license [7,11]. The study-specific annotation subset, source-file identifiers and checksums, derived data, statistical outputs, and analysis and verification code are available from the corresponding author, Dongsun Shin (sdssoft@naver.com), upon reasonable request.

Acknowledgments: The author acknowledges the teams responsible for generating, proofreading, annotating, and publicly releasing the male CNS connectome and its associated data resources.

Conflicts of Interest: The author declares no conflicts of interest.

Declaration of Generative AI and AI-Assisted Technologies: ChatGPT (OpenAI; accessed 2 October 2026) assisted with manuscript revision and the development and execution of analysis and plotting code. All quantitative results were calculated from the supplied source data; the scientific figures were generated programmatically from those measurements. The authors take responsibility for the submitted content.

References

1. Sakurai, T.; Mitsuno, H.; Mikami, A.; Uchino, K.; Tabuchi, M.; Zhang, F.; Sezutsu, H.; Kanzaki, R. Targeted disruption of a single sex pheromone receptor gene completely abolishes in vivo pheromone response in the silkmoth. *Sci. Rep.* **2015**, *5*, 11001. [CrossRef] [PubMed]
2. Kimura, K.-I.; Ote, M.; Tazawa, T.; Yamamoto, D. Fruitless specifies sexually dimorphic neural circuitry in the Drosophila brain. *Nature* **2005**, *438*, 229–233. [CrossRef] [PubMed]
3. Rideout, E.J.; Dornan, A.J.; Neville, M.C.; Eadie, S.; Goodwin, S.F. Control of sexual differentiation and behavior by the doublesex gene in Drosophila melanogaster. *Nat. Neurosci.* **2010**, *13*, 458–466. [CrossRef] [PubMed]
4. Cachero, S.; Ostrovsky, A.D.; Yu, J.Y.; Dickson, B.J.; Jefferis, G.S.X.E. Sexual dimorphism in the fly brain. *Curr. Biol.* **2010**, *20*, 1589–1601. [CrossRef] [PubMed]
5. Dorkenwald, S.; Matsliah, A.; Sterling, A.R.; Schlegel, P.; Yu, S.-C.; McKellar, C.E.; Lin, A.; Costa, M.; Eichler, K.; Yin, Y.; et al. Neuronal wiring diagram of an adult brain. *Nature* **2024**, *634*, 124–138. [CrossRef] [PubMed]
6. Schlegel, P.; Yin, Y.; Bates, A.S.; Dorkenwald, S.; Eichler, K.; Brooks, P.; Han, D.S.; Gkantia, M.; Dos Santos, M.; Munnelly, E.J.; et al. Whole-brain annotation and multi-connectome cell typing of Drosophila. *Nature* **2024**, *634*, 139–152. [CrossRef] [PubMed]
7. Berg, S.; Beckett, I.R.; Costa, M.; Schlegel, P.; Januszewski, M.; Marin, E.C.; Nern, A.; Preibisch, S.; Qiu, W.; Takemura, S.-Y.; et al. Sexual dimorphism in the complete Drosophila male central nervous system connectome. *Cell* **2026**, *189*, 5504–5526.e15. [CrossRef] [PubMed]
8. Schneider-Mizell, C.M.; Gerhard, S.; Longair, M.; Kazimiers, T.; Li, F.; Zwart, M.F.; Champion, A.; Midgley, F.M.; Fetter, R.D.; Saalfeld, S.; et al. Quantitative neuroanatomy for connectomics in Drosophila. *eLife* **2016**, *5*, e12059. [CrossRef] [PubMed]
9. Truman, J.W.; Riddiford, L.M. Drosophila postembryonic nervous system development: A model for the endocrine control of development. *Genetics* **2023**, *223*, iyac184. [CrossRef] [PubMed]
10. Heisenberg, M.; Heusipp, M.; Wanke, C. Structural plasticity in the Drosophila brain. *J. Neurosci.* **1995**, *15*, 1951–1960. [CrossRef] [PubMed]
11. MaleCNS Project. Download the Dataset: Male-CNS v1.0. Available online: https://male-cns.janelia.org/download/ (accessed on 2 October 2026).
12. Lazic, S.E. The problem of pseudoreplication in neuroscientific studies: Is it affecting your analysis? *BMC Neurosci.* **2010**, *11*, 5. [CrossRef] [PubMed]
13. Papke, L.E.; Wooldridge, J.M. Econometric methods for fractional response variables with an application to 401(k) plan participation rates. *J. Appl. Econom.* **1996**, *11*, 619–632. [CrossRef]
14. Virtanen, P.; Gommers, R.; Oliphant, T.E.; Haberland, M.; Reddy, T.; Cournapeau, D.; Burovski, E.; Peterson, P.; Weckesser, W.; Bright, J.; et al. SciPy 1.0: Fundamental algorithms for scientific computing in Python. *Nat. Methods* **2020**, *17*, 261–272. [CrossRef] [PubMed]

Disclaimer/Publisher's Note: The statements, opinions and data contained in all publications are solely those of the individual author(s) and contributor(s) and not of MDPI and/or the editor(s). MDPI and/or the editor(s) disclaim responsibility for any injury to people or property resulting from any ideas, methods, instructions or products referred to in the content.